Antitumor Agents. 152.† *In Vitro* Inhibitory Activity of Etoposide Derivative NPF Against Human Tumor Cell Lines and a Study of Its Conformation by X-ray Crystallography, Molecular Modeling, and NMR Spectroscopy

Yi-Lin Zhang,‡ Alexander Tropsha,*,§ Andrew T. McPhail,⊥ and Kuo-Hsiung Lee*,‡

Natural Products Laboratory and Laboratory for Molecular Modeling, Division of Medicinal Chemistry and Natural Products, School of Pharmacy, University of North Carolina, Chapel Hill, North Carolina 27599, and X-Ray Structure Center, Department of Chemistry, Duke University, Durham, North Carolina 27706

Received November 12, 1993®

NPF, the title compound, was studied for its *in vitro* antitumor activity against 56 human tumor cell lines derived from seven cancer types. In general, NPF is about 100 times more active as compared to its parent compound, etoposide, toward all the tumor cell lines and can be considered as a lead structure for further development of anticancer agents. In order to facilitate future computer-assisted design of NPF analogs, NPF was characterized by X-ray crystallography. This crystal structure was used as the starting point for conformational analysis of this compound using several commercially available software packages, including SYBYL (Tripos Associates; Tripos force field), INSIGHT/DISCOVER (Biosym Technologies; CVFF force field), and semiempirical package MOPAC as implemented in SYBYL. The lowest energy conformation generated with the Tripos force field disagreed with the X-ray structure. On the other hand, semiempirical MOPAC/AM1 calculations showed that the X-ray structure had a lower energy than the Tripos lowest energy conformation. Subsequent NMR studies agreed well with the X-ray structure. Furthermore, conformational analysis of NPF using the DISCOVER force field identified the X-ray structure as the lowest energy conformation. Thus, the latter force field is adequate for future molecular modeling of NPF and its analogs.

Introduction

Etoposide (1, Figure 1) is a widely used anticancer drug which shows good clinical effects against several types of tumors, including testicular and small-cell lung cancers, lymphoma, leukemia, and Kaposi's sarcoma.[2] In order to obtain better antitumor activities and to overcome the problems of development of leucopenia, drug resistance, and poor water solubility, we have engaged in modification of the epipodophyllotoxin structure to develop novel analogs of 1 as potential antitumor agents. Large numbers and varieties of C(4) nonsugar-substituted analogs of 1 have been synthesized, and many have shown greater activity than 1 in inhibiting human DNA topoisomerase II and in forming cellular protein–DNA complexes.[3-11] Among the analogs synthesized in our laboratory, NPF (Figure 1, **2**, 4′-*O*-demethyl-4β-(4″-fluoroanilino)-4-desoxypodophyllotoxin, NSC-628679) is one of the most active compounds, demonstrating 10-fold more potency than 1 in inhibiting human DNA topoisomerase II and 113% more activity than 1 in cellular protein–DNA complex formation.[8] Compound **2** also shows good activity against KB cells and their 1-resistant and vincristin-resistant KB variants which show decreased cellular uptake of 1 and a decrease in DNA topoisomerase II content or an overexpression of MDR1 phenotype.[12] Due to its outstanding enzymatic and KB cell activity, **2** has been submitted to the National Cancer Institute for testing in the *in vitro* human tumor cell line assay and has proven to be very active. Recently, **2** has been selected by the National Cancer Institute for extensive preclinical study

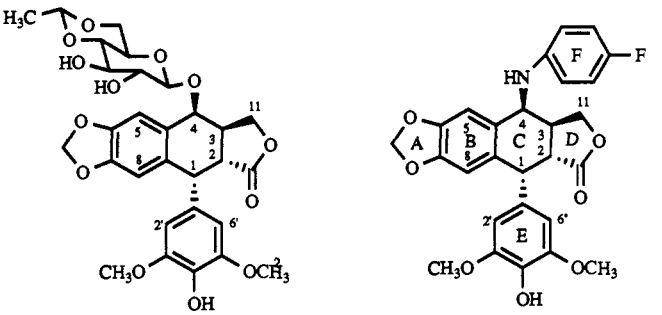

Figure 1.

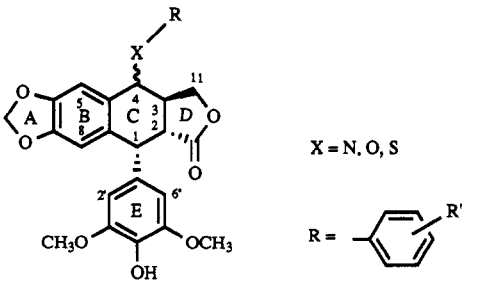

Figure 2.

as a candidate for clinical trials. In order to understand the structure–activity relationships of the synthesized analogs and to facilitate further design, we have initiated molecular modeling studies of novel compounds developed in our laboratory. Due to its important antitumor potential and because it is representative of the structure of the C(4) anilino derivatives of epipodophyllotoxins, we have selected **2** as the lead structure for these studies. The structures of NPF and its close analogs (Figure 2) feature rotatable bond linkages between the A,B,C,D ring system

* To whom correspondence should be addressed.
† For part 151, see ref 1.
‡ Natural Products Laboratory.
§ Laboratory for Molecular Modeling.
⊥ X-Ray Structure Center.
® Abstract published in *Advance ACS Abstracts*, April 1, 1994.

0022-2623/94/1837-1460$04.50/0

Table 1. $\log_{10}$ GI50, $\log_{10}$ TGI, and $\log_{10}$ LC_{50} Mean Graph Midpoints (MG–MID) of Nine Individual *in Vitro* Inhibitory Activity Tests for NPF Against 56 Human Tumor Cell Lines Derived from Leukemia, Non-Small-Cell Lung Cancer, Small-Cell Lung Cancer, Colon Cancer, CNS Cancer, Melanoma, Ovarian Cancer, and Renal Cancer[a]

	test										
	1	2	3	4	5	6	7	8	9	average	etoposide[b]
$\log_{10}$ GI50	−5.96	−6.09	−5.85	−6.15	−5.87	−6.18	−6.06	−6.19	−6.09	−6.05	−4.08
$\log_{10}$ TGI	−5.01	−4.91	−5.02	−6.00	−4.96	−6.01	−4.92	−6.01	−5.06	−5.32	
$\log_{10}$ LC_{50}	−4.21	−4.18	−4.21	−6.00	−4.20	−6.00	−4.10	−6.00	−4.21	−4.79	

[a] GI50: drug concentration (mole, same below) causing 50% cell growth inhibition. TGI: drug concentration causing total cell growth inhibition (0% growth). LC_{50}: drug concentration causing 50% cell death (−50% growth). MG–MID: mean graph midpoints, the average sensitivity of all 56 cell lines in each individual test to the test agent. [b] Data from the National Cancer Institute.

and both the C(4) substituents and the pendant E ring, so the determination of the active conformation of these compounds becomes crucial for future computational molecular modeling studies. Herein, we report the *in vitro* activities of **2** against the human tumor cell lines and the detailed conformational studies of **2** by X-ray crystallography, molecular modeling, and NMR spectroscopy. These extensive studies shall provide the basis for further molecular modeling studies of NPF analogs.

Results and Discussion

Cytotoxicity. The *in vitro* activity of **2** against a total of 56 human tumor cell lines derived from seven cancer types (leukemia, non-small-cell lung cancer, small-cell lung cancer, colon cancer, CNS cancer, melanoma, ovarian cancer, and renal cancer) has been determined in nine separate trials. In each test, dose–response curves for each cell line were measured with five different drug concentrations and the concentration causing 50% cell growth inhibition (GI50), total cell growth inhibition (TGI, 0% growth), and 50% cell death (LC_{50}, −50% growth) compared with the control was calculated. Good reproducibility was found, and the mean graph of GI50 in one representative test is shown in the supplementary material, Figure S1. In this specific test, the mean logarithmic value of GI50 in all cell lines is −6.09; this value is the midpoint of the bar graph. Bars extending to the right represent sensitivity of the cell line to the test agent in excess of the average sensitivity of all tested cell lines. The bar scale is logarithmic; therefore, a bar 2 units to the right (e.g., in the case of P388 leukemia cell line, SN12K1 renal cancer cell line, and NCI-H460 non-small-cell lung cancer) shows the compound achieved the GI50 for the cell line at a concentration one-hundredth the mean concentration required over all cell lines. Thus, the cell line is unusually sensitive to the compound. Bars extending to the left correspondingly imply sensitivity less than the mean. The mean graph midpoint values of $\log_{10}$ GI50, $\log_{10}$ TGI, and $\log_{10}$ LC_{50} of all nine tests are listed in Table 1. The average mean $\log_{10}$ GI50 for all nine tests for **2** is −6.05. Compared with **1** which has a mean $\log_{10}$ GI50 of −4.08 (see supplementary material, Figure S2), **2** is 100-fold more active toward all the tumor cell lines. From the pattern of the mean graph, it is clear that **2** is especially active against leukemia, non-small-cell lung cancer, and renal cancer cell lines. Compound **2** also demonstrated a greater than average activity toward some of the CNS cancer cell lines. On the other hand, compound **2** is less active against ovarian cancer cell lines, melanoma cell lines, and colon cancer cell lines. This activity spectrum is similar to that of **1** but with a 100-fold increase in activity toward all tumor cell lines, including drug-resistant cell lines such as P388/ADR ($\log_{10}$ GI50 of **2** = −7.02, $\log_{10}$ GI50 of **1** = −4.2; data of **1** not shown). Together with the activity toward

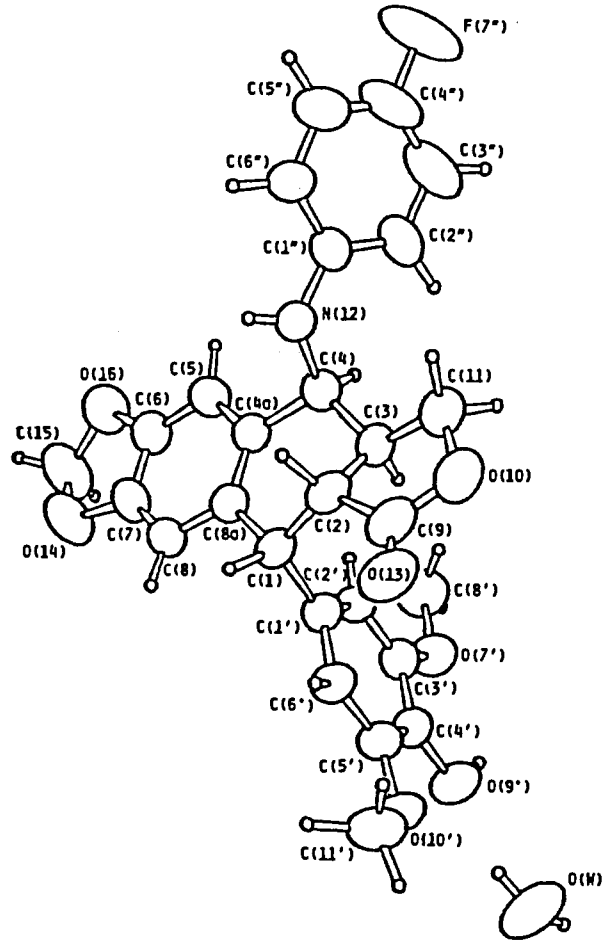

Figure 3. X-ray crystal structure of NPF monohydrate. ORTEP diagram (50% probability ellipsoids) showing the atom-numbering scheme and solid-state conformation of NPF in crystals of the monohydrate; small circles represent hydrogen atoms.

1-resistant KB cells mentioned above, **2** shows great potential for further development.

X-ray Structure Determination. We have determined the X-ray crystal structure of **2** monohydrate (Figure 3) and used this X-ray conformation as the starting point for molecular modeling studies. The torsion angles of C(4)–N(12)–C(1″)–C(2″), C(3)–C(4)–N(12)–C(1″), and C(2)–C(1)–C(1′)–C(2′) were −18.8°, 102.1°, and −85.1°, respectively. Thus, the F ring stretches out from the A,B,C,D ring system, and the E ring plane is nearly perpendicular to the plane of the A,B,C,D ring system as shown in Figure 3. (The crystallographic data are provided in the supplementary material, Tables S1–S5.)

Molecular Modeling Studies of NPF with the Tripos Force Field. After optimizing the X-ray structure with the Tripos force field[13] (Table 2, conformation CNF-1), a systematic search was performed with three rotatable bonds, C(1)–C(1′), C(4)–N(12), and N(12)–C(1″) (see

Table 2. Energy of Different NPF Conformations Calculated by Different Calculation Methods

conformation	description	*E* calculation method	charge method	energy (kcal/mol)
CNF-0	X-ray, no minimization	Tripos	Del Re	149.73
CNF-1	X-ray CNF-0 after Tripos energy minimization	Tripos	Del Re	31.113
CNF-2	Tripos search-generated min.-energy conformation	Tripos	Del Re	29.611
CNF-1	X-ray CNF-0 after Tripos energy minimization	Tripos	Pullman	30.499
CNF-2	Tripos search-generated min.-energy conformation	Tripos	Pullman	26.409
CNF-0	X-ray, no minimization	Tripos	AM1	138.711
CNF-1	X-ray CNF-0 after Tripos energy minimization	Tripos	AM1	22.300
CNF-2	Tripos search-generated min.-energy conformation	Tripos	AM1	19.925
CNF-1	X-ray CNF-0 after Tripos energy minimization	Tripos	no charges	27.302
CNF-2	Tripos search-generated min.-energy conformation	Tripos	no charges	24.099
CNF-0	X-ray, no minimization	AM1	AM1	−176.31[a]
CNF-1	X-ray CNF-0 after Tripos energy minimization	AM1	AM1	−76.76[a]
CNF-2	Tripos search-generated min.-energy conformation	AM1	AM1	−75.14[a]
CNF-3	X-ray CNF-1 after AM1 full geometry optimization	AM1	AM1	−208.89[a]
CNF-4	search CNF-2 after AM1 full geometry optimization	AM1	AM1	−205.14
CNF-0	X-ray, no minimization	Discover	Discover	180.66
CNF-1	X-ray CNF-0 after Tripos energy minimization	Discover	Discover	232.88
CNF-2	Tripos search-generated min.-energy conformation	Discover	Discover	284.90
CNF-5	CNF-1 after Discover energy minimization	Discover	Discover	172.68
CNF-6	CNF-2 after Discover energy minimization	Discover	Discover	175.53
CNF-7	Biosym local minimum	Discover	Discover	173.50

[a] Heat of formation.

Figure 3). The charges were calculated using the Del Re or Pullman methods as well as using the AM1 Hamiltonian of MOPAC as implemented in SYBYL;[13] additional calculations were performed using no charges at all (Table 2). In all four cases, the lowest energy conformation generated by the systematic search (conformation CNF-2) had a different geometry than the X-ray structure (CNF-1): although the A,B,C,D ring system and the E ring overlapped almost exactly, the F ring stretched out from the A,B,C,D ring system in the crystallographic CNF-1 but folded back over the A,B,C,D ring system in CNF-2 (Figure 4). Furthermore, although the energy values varied, the tendency was always the same, with the energy of the search-generated CNF-2 being 1.5–4 kcal/mol lower than that of the X-ray CNF-1.

Since molecular mechanics force fields in principle are parametrized to yield the accurate molecular structures, we felt uncomfortable with this discrepancy in the geometry of the X-ray CNF-1 and the search-generated lowest energy conformation CNF-2. However, this discrepancy may have resulted from packing effects in the crystal structure of NPF that may have not been reproduced by molecular mechanics calculations on a single NPF molecule. To test this hypothesis, we have characterized the NPF structure by NMR in solution as discussed below.

NMR Structure Assignment. A NOESY spectrum of **2** showed no NOE cross-peaks between 2′-H and 8-H or between 2″-H and 11-H. However, a cross-peak between 2″-H and 4-H was observed. In order to confirm that this

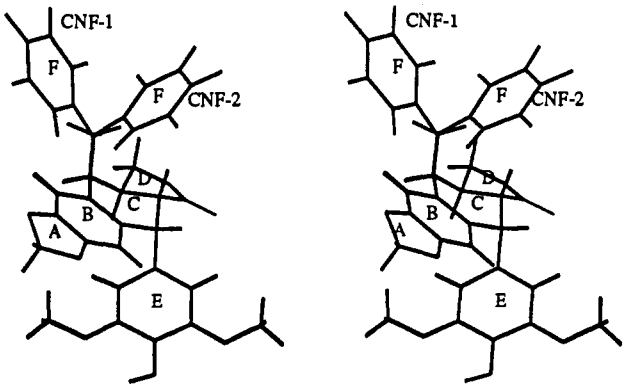

Figure 4. Stereoplot of superimposed conformations CNF-1 (the X-ray conformation) and CNF-2 (the SYBYL search-generated conformation) of NPF. The A–E rings of both conformations superimpose almost exactly. However, the F ring stretches out from the A,B,C,D ring system in the X-ray conformation but folds back over the A,B,C,D ring system in the search-generated conformation.

is due to NOE, we performed a difference NOE experiment. The 4-H and 1-H overlap in the ^{1}H-NMR spectrum and appear at d 4.60 (δ, 2H). The difference NOE spectrum is shown in Figure 5. With irradiation at δ 4.60, NOE peaks appear at δ 6.75 (s, 1H, 5-H and 4-H NOE peak), 6.53 (s, 1H, 8-H and 1-H NOE peak), and 6.49 (q, J = 2.2, 6.2 Hz, 2H, 2″- or 6″-H and 4-H NOE peak). The distance between 2″-H and 4-H is 1.98 Å in the X-ray structure of NPF (CNF-1) and 4.07 Å in the search-generated minimum-energy conformation (CNF-2). Because a NOE is

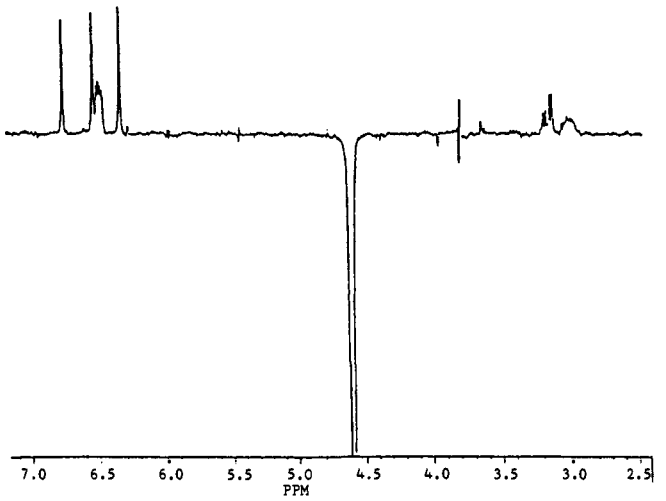

Figure 5. Difference NOE spectrum of NPF.

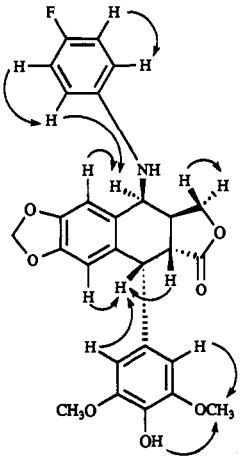

Figure 6. NOE correlation of NPF (2).

observed only between spatially close hydrogens, the finding of a NOE between 2″-H and 4-H suggests that the F ring stretches out from the A,B,C,D ring system instead of folding over it. The NOE correlation of **2** is shown in Figure 6. Thus, from the NMR information, we conclude that the conformation with the F ring stretching out of the A,B,C,D ring system is favored in solution as well as in the crystal structure.

Choosing the Appropriate Molecular Modeling Tool. The discrepancy between the lowest energy conformation of NPF generated with the Tripos force field and the NPF structure determined with X-ray and NMR led us to believe that the Tripos force field may be inadequate for modeling this compound and its close analogs. Further support for this conclusion came when we performed full geometry optimization of both crystallographic CNF-1 and Tripos-generated CNF-2 structures using semiempirical MOPAC/AM1 calculations. The resulting heat of formation for geometry-optimized CNF-1 was ca. 3.5 kcal/mol lower than that of the geometry-optimized CNF-2 (cf. CNF-3 and CNF-4, Table 2). We also noticed that even the heat of formation of the X-ray structure (CNF-0) was much lower than that of both the Tripos energy-minimized X-ray structure (CNF-1) and the lowest energy search conformation (CNF-2; cf. Table 2). The resulting conformation (CNF-3) looked similar to CNF-1 (e.g., F ring stretching out), whereas CNF-4 was similar to CNF-2. These data indicate that although the conformational search with the Tripos force field may have

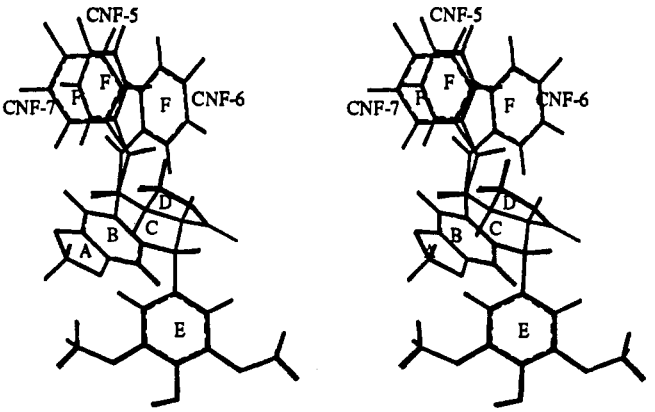

Figure 7. Stereoplot of superimposed conformations CNF-5, CNF-6, and CNF-7 generated with the systematic conformational search using CVFF force field. Conformations CNF-5, CNF-6, and CNF-7 are the same as described in Table 2.

identified a (possible) low-energy conformation, it is not observed, however, either in crystals or in solution.

The MOPAC/AM1 model thus appears more suitable for accurate description of the molecular geometry of NPF. Unfortunately, the routine application of semiempirical calculations as a conventional conformational analysis and drug-design tool is still limited due to inadequate computer power, whereas molecular mechanics-based methods are much faster and therefore more efficient, provided that they are accurate. Thus, we have tested the ability of a different force field, CVFF as implemented in the Biosym Modeling Software INSIGHT/DISCOVER,[14] to reproduce the crystallographic and NMR geometry of NPF. Interestingly, even single-point energy calculations with the CVFF force field on the X-ray CNF-0, the Tripos geometry-optimized X-ray CNF-1, and the lowest energy CNF-2 conformers showed immediately that the CNF-0 conformation was of lower energy (cf. Table 2). Further geometry optimization of both molecules with the conjugate gradient minimization scheme and the 0.01-rms deviation convergence criterion generated conformations CNF-5 and CNF-6, respectively (Table 2). The geometry of the former conformer was still very similar to that of the initial X-ray structure CNF-0, whereas the orientation of the pendant E ring with respect to the A,B,C,D ring system in CNF-6 changed drastically toward a more unfolded, "stretched-out" conformation as in the X-ray structure (see below). Furthermore, the CNF-5 conformer was also ca. 3 kcal/mol lower in energy. Finally, we performed a systematic conformational search around the C(4)–N(12) and N(12)–C(1″) (Figure 3) rotatable bonds (5° increments, 10 kcal/mol energy window above the lowest energy conformation, and energy minimization of each conformation), starting from the energy-minimized X-ray conformation CNF-5. This search yielded three low-energy conformations of NPF (Figure 7), including the X-ray conformation (CNF-5) which still had the lowest energy (Table 2). Another local minimum-energy conformation actually matched the CNF-6 conformation produced by optimizing the geometry of the Tripos lowest energy search conformation CNF-2 with the CVFF force field (Table 2 and Figure 7), and the third conformation had a somewhat different orientation of the F ring. These results indicate that the two force fields describe different potential energy surfaces for the NPF molecule and that the Tripos lowest energy conformation is not considered by the CVFF force field even as a local minimum. Remarkably, the CVFF force field was

able to identify the X-ray and the NMR conformation of NPF as the most stable one.

Conclusions and Prospectus

Using a variety of experimental and computational techniques, we have studied an etoposide derivative, NPF, which is a lead compound for further anticancer drug-design studies. In order to develop an adequate molecular model of NPF, we have tested the ability of two force fields, Tripos and CVFF, to reproduce the experimental, X-ray, and NMR-determined conformations of NPF. The calculation using the former force field failed to identify the experimentally determined conformation as the lowest energy structure, whereas the lowest energy conformation found with the CVFF force field was in excellent agreement with the experimental structure. We suggest that the Biosym CVFF force field is an adequate tool for modeling NPF and its structural analogs, and it shall be utilized in future molecular modeling studies of this class of compounds.

Experimental Methods

1. Biological Assay. NPF was tested in different concentrations against every cell line. All lines were inoculated onto a series of standard 96-well microtitre plates on day 0, in the majority of cases at 20 000 cells/well, and then preincubated in the absence of drug for 24 h. NPF was then added in five 10-fold dilutions, and the cells were incubated for a further 48 h. Following this, the cells were fixed *in situ*, washed, and dried. SRB was added followed by further washing and drying of the stained adherent cell mass. The bound stain was solubilized and measured spectrophotometrically on an automatic plate reader. The biological assays were performed by the National Cancer Institute. Literature describing the *in vitro* human tumor cell line assay is available.[15-16]

2. X-ray Crystallography. The crystal structure was solved by direct methods (MULTAN11/82). Initial non-hydrogen-atom positions were derived from an E-map. Hydrogen atoms were located in a series of difference Fourier syntheses evaluated following several rounds of full-matrix least-squares adjustment of non-hydrogen-atom positional and thermal parameters (at first isotropic and then anisotropic), and their positional and isotropic thermal parameters were included as variables in the subsequent least-squares iterations. An extinction correction was also refined during the final cycles. The parameter refinement converged at $T = 0.038$ ($R_w = 0.053$). A final difference Fourier synthesis contained no unusual features.

Crystallographic calculations were performed on PDP11/44 and Micro-VAX computers using the Enraf-Nonius Structure Determination Package (SDP). For all structure-factor calculations, neutral atom-scattering factors and their anomalous dispersion corrections were taken from *International Tables for X-Ray Crystallography*; The Kynoch Press, Birmingham, England, 1974; Vol. IV.

3. Molecular Modeling. The molecular modeling study was performed using SYBYL 5.5[13] and INSIGHT/DISCOVER 2.0.2[14] on the ESV and IBM RISC6000 workstations in the Laboratory for Molecular Modeling. The atomic charges were calculated with the Del Re and Pullman methods as well as with the semiempirical molecular orbital program MOPAC,[17] version 4.10, using the AM1 (Austin Method 1)[18] Hamiltonian as implemented in SYBYL. Systematic searches were performed with 5° angle increments; the SYBYL default VDW factors were reduced to 0.71 (general factor), 0.5 (H-bond), and 0.69 (one–four VDW), and the default INSIGHT/DISCOVER VDW factors were used.

4. NMR. The NMR spectrum was taken on a Bruker AC 300-MHz NMR. $CDCl_3$ was used as the solvent and TMS as the internal standard. The chemical shifts (δ) were expressed as parts per million.

Acknowledgment. This work was supported by grants from the American Cancer Society, DHP-13 E and -13 F (K. H. Lee). We acknowledge TRIPOS Associates, Inc., and Biosym Technologies, Inc., for the software grants. The authors also thank Dr. Yoshiki Kashiwada for helping with the measurements of the NMR spectra, Professor Iosif Vaisman for fruitful discussions, and anonymous reviewers for helpful critique and for editing the manuscript.

Supplementary Material Available: Data tables for NPF monohydrate and mean bar graphs of $\log_{10}$ GI50 of NPF and etoposide (13 pages). Ordering information is given on any current masthead page.

References

(1) Chen, C. H.; Yang, L. M.; Lee, T. T.; Shen, Y. C.; Zhang, D. C.; Pan, D. J.; McPhail, A. T.; McPhail, D. R.; Liu, S. Y.; Li, D. H.; Cheng, Y. C.; Lee, K. H. Antitumor Agents 151. Bis(helenalinyl)glutarate and Bis(Isoalantodiol-B)glutarate, Potent Inhibitors of Human DNA Topoisomerase II. *Bioorg. Med. Chem.*, in press.
(2) O'Dwyer, P. J.; Leyland-Jones, B.; Alonso, M. T.; Marsoni, S.; Wittes, R. E. Etoposide (VP-16-213): Current Status of an Active Anticancer Drug. *N. Engl. J. Med.* **1985**, *312*, 692–700.
(3) Zhang, Y. L.; Shen, Y. C.; Wang, Z. Q.; Chen, H. X.; Guo, X.; Cheng, Y. C.; Lee, K. H. Antitumor Agents, 130. Novel 4β-arylamino Derivatives of 3′,4′-Didemethoxy-3′,4′-dioxo-4-deoxypodophyllotoxin as Potent Inhibitors of Human DNA Topoisomerase II. *J. Nat. Prod.* **1992**, *55*, 1100–1111.
(4) Wang, Z. Q.; Hu, H.; Cheng, H. X.; Cheng, Y. C.; Lee, K. H. Antitumor Agents. 124. New 4β-Substituted Aniline Derivatives of 6,7-*O*,*O*-Demethylene-4′-*O*-demethylpodophyllotoxin and Related Compounds as Potent Inhibitors of Human DNA Topoisomerase II. *J. Med. Chem.* **1992**, *35*, 871–877.
(5) Hu, H.; Wang, Z. Q.; Liu, S. Y.; Cheng, Y. C.; Lee, K. H. Antitumor Agents. 123. Synthesis and Human DNA Topoisomerase II Inhibitory Activity of 2′-Chloro Derivatives of Etoposide and 4β-(Arylamino)-4′-*O*-demethylpodophyllotoxins. *J. Med. Chem.* **1992**, *35*, 867–871.
(6) Zhou, X. M.; Wang, Z. Q.; Chang, J. Y.; Chen, H. X.; Cheng, Y. C.; Lee, K. H. Antitumor Agents. 120. New 4-Substituted Benzylamine and Benzyl Ether Derivatives of 4′-*O*-Demethylepipodophyllotoxin as Potent Inhibitors of Human DNA Topoisomerase II. *J. Med. Chem.* **1991**, *34*, 3346–3350.
(7) Wang, Z. Q.; Kuo, Y. H.; Schnur, D.; Bowen, J. P.; Liu, S. Y.; Han, F. S.; Chang, J. Y.; Cheng, Y. C.; Lee, K. H. Antitumor Agents. 113. New 4β-Arylamino Derivatives of 4′-*O*-Demethylpodophyllotoxin and Related Compounds as Potent Inhibitors of Human DNA Topoisomerase II. *J. Med. Chem.* **1990**, *33*, 2660–2666.
(8) Lee, K. H.; Beers, S. A.; Mori, M.; Wang, Z. Q.; Kuo, Y. H.; Li, L.; Liu, S. Y.; Chang, J. Y.; Han, F. S.; Cheng, Y. C. Antitumor Agents. 111. New 4-Hydroxylated and 4-Halogenated Anilino Derivatives of 4′-Demethylepipodophyllotoxin as Potent Inhibitors of Human DNA Topoisomerase II. *J. Med. Chem.* **1990**, *33*, 1364–1368.
(9) Lee, K. H.; Imakura, Y.; Haruna, M.; Beers, S. A.; Thurston, L. S.; Dai, H. J.; Chen, C. H.; Liu, S. Y.; Cheng, Y. C. Antitumor Agents. 107. New Cytotoxic 4-Alkylamino Analogues of 4′-Demethylepipodophyllotoxin as Potent Inhibitors of Human DNA Topoisomerase II. *J. Nat. Prod.* **1989**, *52*, 606–613.
(10) Thurston, L. S.; Imakura, Y.; Haruna, M.; Li, D. H.; Liu, Z. C.; Liu, S. Y.; Cheng, Y. C.; Lee, K. H. Antitumor Agents. 100. Inhibition of Human DNA Topoisomerase II by Cytotoxic Ether and Ester Derivatives of Podophyllotoxin and α-Peltatin. *J. Med. Chem.* **1989**, *32*, 604–608.
(11) Beers, S. A.; Imakura, Y.; Dai, H. J.; Cheng, Y. C.; Lee, K. H. Antitumor Agents. 99. Synthetic Ring C Aromatized Podophyllotoxin Analogues as Potent Inhibitors of Human DNA Topoisomerase II. *J. Nat. Prod.* **1988**, *51*, 901–905.
(12) Chang, J. Y.; Han, F. S.; Liu, S. Y.; Wang, Z. Q.; Lee, K. H.; Cheng, Y. C. Effect of 4β-Arylamino Derivatives of 4′-*O*-Demethylepipodophyllotoxin on Human DNA Topoisomerase II, Tubulin Polymerization, KB Cells, and Their Resistant Variants. *Cancer Res.* **1991**, *51*, 1755–1759.
(13) SYBYL, version 5.5; Tripos Associates, Inc.: St. Louis, MO, 1992.
(14) *Insight II User Guide, Version 2.1.0*; Biosym Technologies: San Diego, 1992.
(15) Boyd, M. R. Status of the NCI Preclinical Antitumor Drug Discovery Screen. *Princ. Pract. Oncol.* **1989**, *3* (10), 1–12.
(16) Paull, K. D.; Shoemaker, R. H.; Hodes, L.; Monks, A.; Scudiero, D. A.; Rubinstein, L.; Plowman, J.; Boyd, M. R. Display and Analysis of Patterns of Differential Activity of Drugs Against Human Tumor Cell Lines: Development of Mean Graph and COMPARE Algorithm. *J. Natl. Cancer Inst.* **1989**, *81*, 1088–1092.
(17) Stewart, J. J. P. MOPAC: A Semiempirical Molecular Orbital Program. *J. Comput.-Aided Mol. Des.* **1990**, *4*, 1–105.
(18) Dewar, M. J. S.; Zoebisch, E. F.; Healey, E. F.; Stewart, J. J. P. AM1: A New General Purpose Quantum Mechanical Molecular Model. *J. Am. Chem. Soc.* **1985**, *107*, 3902–3909.